ELSEVIER

Surface Science 366 (1996) 323–336

surface science

Reactive oxygen sites at MoO_3 surfaces: ab initio cluster model studies

A. Michalak [a], K. Hermann [b,*], M. Witko [c]

[a] *Department of Computational Methods in Chemistry, Faculty of Chemistry, Jagiellonian University, R. Ingardena 3, 30060 Cracow, Poland*

[b] *Fritz-Haber-Institut der Max-Planck-Gesellschaft, Faradayweg 4–6, D-14195 Berlin, Germany*

[c] *Institute of Catalysis and Surface Chemistry, Polish Academy of Sciences, Niezapominajek, 30239 Cracow, Poland*

Received 25 January 1996; accepted for publication 9 May 1996

Abstract

The electronic structure and bonding of geometrically inequivalent surface oxygens is examined for MoO_3(010) and (100) surfaces where the local electronic structure is obtained from ab initio density functional theory (DFT–LCGTO) cluster calculations. The clusters are chosen as finite sections of the ideal MoO_3 surface where cluster embedding is achieved by bond saturation with hydrogens, yielding clusters up to $Mo_7O_{30}H_{18}$. Local charging, bond orders, and electrostatic potentials of the surface clusters depend weakly on cluster size, suggesting general validity for the extended surface. The difference in electronic structure between the (010) and (100) surface is found to be mainly due to the different atom arrangement, while local atom charging and binding properties are surface-independent. Terminal molybdenyl oxygens experience the smallest negative charging and form double bonds with the adjacent Mo centers. Asymmetric bridging oxygens are slightly more negative and similar in their binding scheme to molybdenyl oxygens. Symmetric bridging oxygens become most negative and form single bonds with the two neighboring Mo centers. Electrostatic potentials determined from cluster charge distributions show broad negative minima above the terminal oxygens while there are no minima above bare Mo metal centers which can affect stabilization and binding of adparticles at the MoO_3 surfaces.

Keywords: Catalysis; Density functional calculations; Molybdenum oxides; Single crystal surfaces

1. Introduction

The physics and chemistry of transition-metal oxides is of considerable interest, both from a technological and a basic scientific point of view. These materials are used in many industrial applications. As examples we mention their use as electrode material in electrochemical processes, as functional components of catalysts for hydrocarbon conversion, or as precursors of catalysts for hydrodesulfurization [1–5]. The specific catalytic properties of transition-metal oxides follow from their ability to easily undergo surface oxidation and reduction, which is usually combined with high densities of cationic and anionic vacancies. The surface ions can form Lewis acid and base sites as well as acid-base pair sites, which influences the electronic structure and affects properties like surface electric field gradients and surface electrostatic potential. Further, transition-metal oxides exist in many different crystallographic forms, with

* Corresponding author. Fax: +49 30 84134701; e-mail: hermann@fhi-berlin.mpg.de

PII S0039-6028(96)00812-6

stoichiometries differing only slightly from each other and transition-metal ions exhibiting various oxidation states [1]. The latter makes their experimental and theoretical study quite difficult and interesting at the same time.

Molybdenum oxides are of great scientific importance since their chemical behavior is very complex and is characterized by a variety of different effects. These oxides, prepared as pure substrates or as compounds including other transition-metal oxides, can act as catalysts in many reactions of different types [5], such as redox processes, acid-base processes (e.g. isomerization, polymerization), hydrogenation and dehydrogenation, selective oxidation and oxidative conversion. (A full list of reactions catalyzed by molybdenum oxides and molybdates can be found in Table 1 of Ref. [5].) In particular, molybdenum trioxide (MoO_3), based materials play an important role as catalysts in the selective oxidation of hydrocarbons due to their structural and electronic surface properties. In experiments, the oxidation is found to involve several steps yielding different products as a function of the local surface geometry and elemental composition of the molybdenum compound [5]. In a first step, an organic molecule is activated by hydrogen abstraction near oxygen surface sites, and in subsequent steps oxygens (possibly from different sites) are inserted. The details of these processes depend on the specific surface orientation. As an example we mention the conversion process

$$\text{propene}(CH_3-CH=CH_2) \rightarrow \text{allyl}(CH_2-CH-CH_2 \rightarrow \text{acroleine}(CH_2=CH-CHO).$$

Here the allyl-to-acroleine conversion (involving simultaneous hydrogen abstraction and oxygen insertion) is found to occur on MoO_3(010) but not on (100) surfaces [5]. On the other hand, direct conversion of propene to acroleine is claimed to happen, however with low selectivity on MoO_3(100) but not on (010) surfaces [6,7]. Experimental as well as theoretical details of these oxidation reactions are still under discussion [5–7], and a microscopic understanding of the electronic structure and binding properties at the different surface oxygen sites is lacking.

In the present theoretical study we examine the electronic structure and bonding of geometrically inequivalent surface oxygens for both (010) and (100) oriented ideal MoO_3 surfaces. Since oxygen binding can be considered a local phenomenon, the surface cluster approach becomes meaningful. Thus, the surface environment about the oxygens is represented by bond-saturated surface clusters of different sizes and shapes. Electronic wavefunctions and respective properties such as local charging, bond character, or electrostatic potentials of the surface clusters, are determined by ab initio density functional theory (DFT) calculations based on linear combinations of Gaussian-type atomic orbitals (LCGTO).

The calculated electronic parameters for a given surface oxygen site show only minor variations with cluster size, which justifies the use of the surface cluster approach for the present systems. Population analyses confirm the ionic nature of the MoO_3 compound, and show pronounced differences for geometrically different surface oxygen sites. The actual ionic charging is found to be smaller than suggested by the formal oxidation states of the atoms, and identifies sizable covalent contributions to the interatomic binding. The electronic structure described by the population analyses is substantiated by respective bond-order indices obtained for the clusters. Electron density distributions about the central cluster atoms (charge-density difference maps) give further support of the interatomic binding mechanisms. Finally, electrostatic potentials computed from the cluster charge distributions can give additional information about binding and local charging. Overall, the present cluster studies give a sound characterization of the electronic structure at MoO_3(010) and (100) surfaces which can be used for detailed studies on adsorbate binding and reactions [8].

In Section 2 we briefly review structural and computational details of the present study, while in Section 3 we present numerical results and discussion for both MoO_3(010) and (100) surface-based clusters. Finally, Section 4 summarizes the

conclusions, stressing those features which are relevant for the real surface situation.

2. Structural and computational details

Molybdenum trioxide (MoO_3) forms an ionic layer type orthorhombic crystal structure [9] where bilayers lie parallel to the (010) netplane, which represents the easy cleavage plane of the crystal (see Fig. 1). The bilayers can be characterized by two sublayers consisting of a periodic arrangement of distorted MoO_6 octahedra where oxygen ions are shared between adjacent octahedra within and between the sublayers (cf. Figs. 2a and 2b). The octahedral units shown in Fig. 2b have Mo–O distances d_{Mo-O} which vary between 3.16 and 4.41 bohr (1.68 and 2.33 Å), where the largest value refers to oxygens shared by neighboring octahedra of different sublayers, and the smallest value is found for oxygens at the top and bottom of the bilayer. While the internal interaction between atoms within the bilayers is dominated by rather strong ionic and covalent bonding, the bilayers couple via weak van der Waals forces.

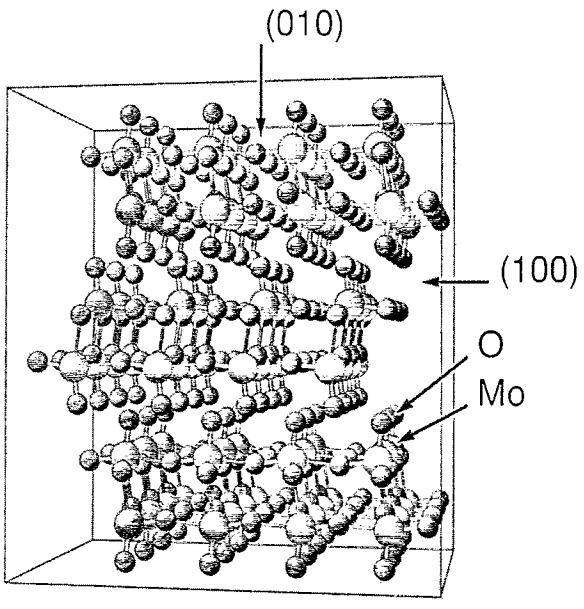

Fig. 1. Perspective view of the orthorhombic MoO_3 crystal lattice. The (010) net plane defines the top of the rectangular crystal section of three bilayers, while the (100) net plane confines the section to the right and the (001) net plane to the front. The Mo and O centers are shown as spheres of different size and shading.

The ideal (010) surface of MoO_3 is characterized by a simple network of Mo and O ions, where there are basically three types of structurally different surface oxygen centers. First, the terminal (molybdenyl) oxygens, denoted O(a) in Fig. 2a, are coordinated to one Mo center directly below at a distance of 3.16 bohr (1.67 Å) and cover all Mo ions at the surface. Second, the asymmetrically bridging oxygens, denoted O(b) ($O(b_1)$ and $O(b_2)$) in Fig. 2a, are coordinated to one Mo center at a distance of 3.28 bohr (1.74 Å) and couple weakly with another surface Mo ($d_{Mo-O}=4.25$ bohr (2.25 Å)). Third, the symmetrically bridging oxygens, O(b′) of Fig. 2a, are coordinated to two Mo centers of the surface at distances of 3.68 bohr (1.95 Å) and couple weakly with a Mo center of the underlying sublayer ($d_{Mo-O}=4.41$ bohr (2.33 Å)).

The ideal (100) surface of MoO_3 is rather different in its structure from the (010) surface (see Fig. 1). This surface is much less compact, i.e. its appearance does not resemble that of a closed planar surface and there are many structurally different metal as well as oxygen sites. The molybdenyl oxygens, O(a) of Fig. 3a, are similar to those of the (010) surface and are coordinated to one Mo center at a distance of 3.28 bohr (1.74 Å). However, these O(a) atoms do not cover all Mo ions, leaving bare metal sites at the (100) surface as opposed to the situation at the (010) surface. The symmetrically bridging oxygens, $O(b'_1)$ and $O(b'_2)$ of Fig. 3a, correspond structurally to the O(b′) atoms of the (010) surface. They are coordinated to two Mo centers, Mo(1), of the surface at distances of 3.68 bohr (1.95 Å), and couple weakly with a third Mo surface center ($d_{Mo-O}=4.41$ bohr (2.33 Å)). Finally, the oxygens $O(d_1)$ and $O(d_2)$ of Fig. 3a correspond structurally to terminal molybdenyl oxygens of the (010) surface. They lie close to the plane of the surface molybdenums and are coordinated to one Mo center at a distance of 3.16 bohr (1.68 Å).

The above description of the MoO_3 crystal structure and of the two different surfaces determines the geometries of local model clusters considered in this study. For the MoO_3(010) surface, the present clusters are shown in Figs. 2b–d. Here the

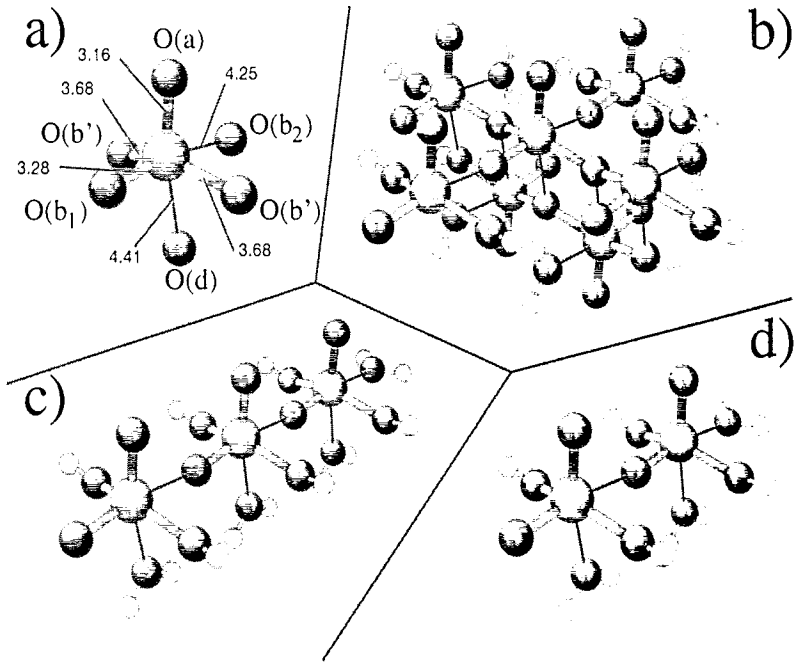

Fig. 2. Clusters used to model the (010) surface of MoO_3. (a) Defines the inequivalent oxygen centers O(a–d) about the central molybdenum in a distorted octahedral MoO_6 environment and lists interatomic distances (in bohr). (b–d) visualize the $Mo_7O_{30}H_{18}$, $Mo_3O_{16}H_{14}$ and $Mo_2O_{11}H_{10}$ clusters used in the present study where peripheral hydrogens providing bond saturation are shown as small white spheres. The coordination of the atom centers is indicated by bond sticks, whose thicknesses denote the amount of coupling between respective centers.

largest cluster, $Mo_7O_{30}H_{18}$ (Fig. 2b), represents a symmetric surface section about a molybdenyl unit such that at least one member of each of the structurally different surface oxygens, O(a), O(b) and O(b'), occurs and experiences its full nearest-neighbor environment within the cluster. In addition, peripheral oxygens are electronically saturated (if needed) by hydrogen atoms, as will be discussed below. The smaller clusters, $Mo_3O_{16}H_{14}$ (Fig. 2c) and $Mo_2O_{11}H_{10}$ (Fig. 2d), are subunits of the largest cluster and are used to examine the cluster-size dependence of electronic parameters. For the MoO_3(100) surface the clusters are shown in Fig. 3b–d. Here the largest cluster, $Mo_6O_{24}H_{12}$ (Fig. 3b), gives a characteristic surface unit where each of the important structurally different surface oxygens, O(a), O(b') and O(d), is represented by a center with its full nearest-neighbor environment within the cluster. In addition, hydrogens serve as bond saturators at the cluster periphery (see below). The $Mo_5O_{19}H_8$ cluster (Fig. 3c) differs from $Mo_6O_{24}H_{12}$ essentially by the missing MoO_5 part modeling the second molybdenum/oxygen "layer" in the largest cluster, and can thus be used to study the influence of electronic coupling perpendicular to the surface. Further, $Mo_3O_{12}H_6$ (Fig. 3d) forms a subunit of the $Mo_5O_{19}H_8$ cluster where atoms parallel to the surface are left out. Therefore, the smallest cluster can be used to obtain information about the influence of electronic coupling parallel to the surface.

The present surface clusters are chosen as finite sections of the ideal MoO_3(010) and (100) surfaces. This assumes that these surfaces do not exhibit major reconstruction, which is suggested from the experiment [3,5]. Further, a meaningful representation of the extended surface by a finite surface cluster requires that the electronic embedding of the cluster into its surface environment is appropriately accounted for. For purely ionic systems Madelung-potential embedding could be used to correct approximately for long-range Coulomb contributions [10], but has not been considered here due to the complexity of the MoO_3 crystal

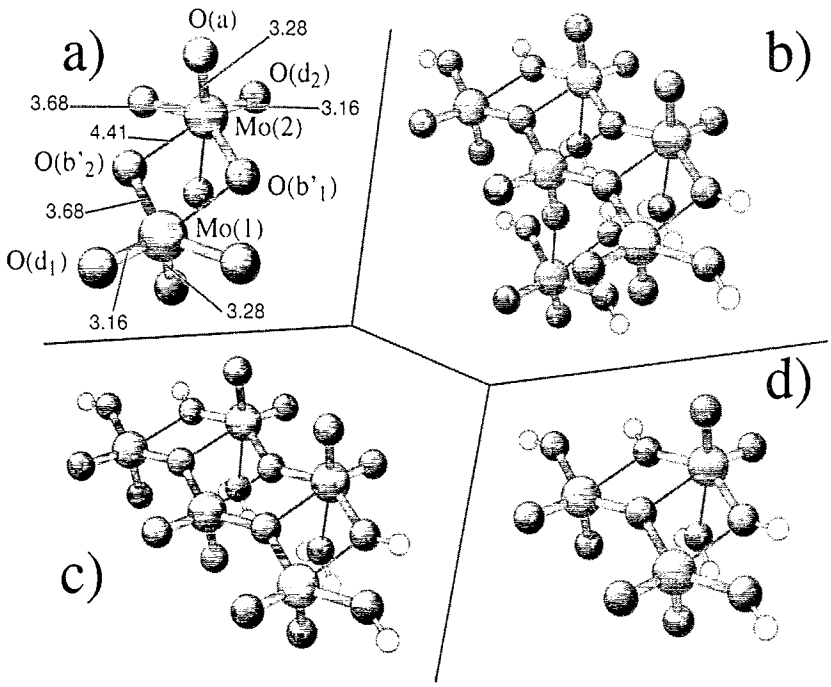

Fig. 3. Clusters used to model the (100) surface of MoO_3. (a) Defines the inequivalent oxygen centers O(a–d) about the two central molybdenums Mo(1) and Mo(2) in the distorted bi-octahedral environment and lists interatomic distances (in bohr). (b–d) visualize the $Mo_6O_{24}H_{12}$, $Mo_5O_{19}H_8$ and $Mo_3O_{12}H_6$ clusters used in the present study, where peripheral hydrogens providing bond saturation are shown as small white spheres. The coordination of the atom centers is indicated by bond sticks whose thicknesses denote the amount of coupling between respective centers.

structure. Alternatively, one can approximate the electronic embedding of the local cluster by saturating all bonds that the peripheral cluster atoms can form with their neighbors at the substrate surface which are missing in the cluster. This latter approach was taken in the present study where all peripheral oxygen atoms were "bond saturated" by adding appropriate hydrogens at a distance $d_{O-H} = 1.83$ bohr (0.97 Å)). Two different saturation schemes were examined. In the first scheme, the number of hydrogens used to saturate a given cluster oxygen is determined by the expected bond strength between this atom and its nearest Mo neighbor in the cluster. Thus, oxygens bound by an Mo=O double bond resulting in the shortest Mo–O distances (3.16 and 3.28 bohr) are assumed to be already fully saturated. Oxygens bound by a Mo–O single bond leading to intermediate Mo–O distances (3.68 bohr) are assumed to require one additional hydrogen for saturation. Finally, weakly bound oxygens reflected by large Mo–O distances (4.25–4.41 bohr) are assumed to require two additional hydrogens for saturation. (These oxygens are strongly bound to molybdenums neglected in the cluster.) This procedure leads for the smallest (010) surface cluster to $Mo_2O_{11}H_{10}$ as shown in Figs. 2d and 4a. In the second saturation scheme, applied in a recent study on small MoO_6H_x clusters [11], the number of hydrogens used to saturate a given cluster oxygen corresponds to the number of its missing molybdenum neighbors in the bulk. This scheme results in a (010) surface cluster $Mo_2O_{11}H_{13}$ (see Fig. 4b), which has to be considered electronically as a positive $Mo_2O_{11}H_{13}^{3+}$ ion in order to comply with the formal oxidation states of the constituent atoms. A comparison of results between the two clusters discussed below and more detailed tests suggest that the first saturation scheme, while being more complicated, leads to smaller cluster-size variations of the electronic parameters. Hence the first scheme seems more reasonable than the second, and is

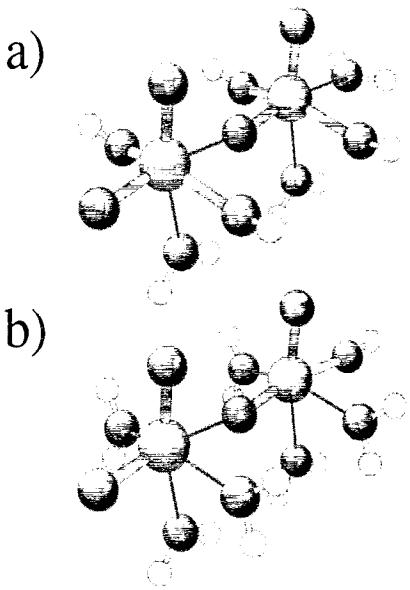

Fig. 4. Geometric structure of (a) the $Mo_2O_{11}H_{10}$ (see also Fig. 2d) and (b) $Mo_2O_{11}H_{13}$ clusters used to simulate different bond saturations of the peripheral oxygens by hydrogens. The saturation hydrogens are shown by small white spheres.

therefore used in all extended calculations of the present study.

The electronic wavefunctions and derived properties of the clusters are determined with the ab initio density functional theory (DFT) method [12] using linear combinations of atomic orbitals with flexible basis sets of contracted Gaussian–type orbitals (LCGTO). The basis sets were taken from DFT optimizations [13] and were all-electron type (double zeta + polarization, DZVP) for all O and H centers, while the Mo centers were represented by a (4s,4p,4d,5s) DZVP valence basis with the $[Ar]3d^{10}$ core described by a model core potential [14]. Further definitions of the basis sets are given in Table 1. In the calculations the program package DeMon [15] was applied using the local spin density approximation (LSDA) for exchange and correlation based on the Vosko–Wilk–Nusair functional [16]. As a result of the peripheral bond saturation only the energetically lowest electronic cluster states have to be considered, and higher-lying ionic states can be neglected [17]. For the cluster analysis the DFT wavefunction was used to determine atom-center charges based on the Mulliken population analysis [18], bond-order indices [19,20], electron charge densities, and electrostatic potential distributions [21].

Table 1
List of the Gaussian orbital and auxiliary basis sets used in the present DFT calculations; the basis sets for oxygen and hydrogen are all-electron type, while the molybdenum basis is used to describe only valence electrons (4s,4p,4d,5sp) with a pseudopotential representing the $Ar/3d^{10}$ electron core; the table contains both the internal basis notation of the DeMon program system and the conventional notation

Atom	Orbital basis		Auxiliary basis	
	DeMon	Conventional	DeMon	Conventional
Mo	(311111/31111/2111)	(8s7p5d/6s5p4d)	(5,5;5,5)	(10s5p5d)
O	(621/41/1*)	(9s5p1d/3s2p1d)	(4,3;4,3)	(7s3p3d)
H	(41)	(5s/2s)	(4;4)	(4s)

3. Results and discussion

3.1. MoO_3(010) *surface based clusters*

Table 2 lists calculated populations and bond orders obtained from the different surface clusters, $Mo_7O_{30}H_{18}$, $Mo_3O_{16}H_{14}$ and $Mo_2O_{11}H_{10}$, repre-

Table 2
Populations and bond orders obtained from clusters representing the MoO_3(010) surface; the geometric structures of the clusters $Mo_7O_{30}H_{18}$, $Mo_3O_{16}H_{14}$, $Mo_2O_{11}H_{10}$ and $Mo_2O_{11}H_{13}$ are shown in Figs. 2b–2d, respectively; the population charges q and bond orders involving molydbenum always refer to the central Mo centers of the clusters; the inequivalent oxygens O(a-d) are defined in Fig. 2a

	$Mo_7O_{30}H_{18}$	$Mo_3O_{16}H_{14}$	$Mo_2O_{11}H_{10}$	$Mo_2O_{11}H_{13}^{3+}$
Populations				
Mo	40.33	40.57	40.69	40.58
O(a)	8.39	8.40	8.43	8.23
O(b)	8.54	8.55	8.54	8.64
O(b′)	8.84	8.76	8.77	8.81
O(d)	8.84	8.81	8.81	8.81
Bond orders				
Mo-O(a)	1.93	1.97	1.95	2.10
Mo-O(b_1)	1.50	1.58	1.58	1.34
Mo-O(b_2)	0.20	0.21	0.16	0.25
Mo-O(b′)	0.66	0.92	0.87	0.45
Mo-O(d)	0.19	0.20	0.20	0.25

senting the $MoO_3(010)$ surface. As a first important result, the data of Table 2 show only little variation between the three different size clusters using the same peripheral bond saturation scheme. This demonstrates that the surface cluster approach applied to the present system is reasonable. Population analyses can be used as a rough guide for the charge redistribution due to interaction and bond formation between the atoms in the clusters. The present data confirm the ionic nature of the MoO_3 compound as suggested by basic chemical intuition. However, the actual ionic charging is found to be smaller than expected, which suggests sizable covalent contributions to the interatomic binding in the clusters. The Mo metal centers become positively charged and can be described as Mo+(1.3–1.7) ions from the populations. The terminal molybdenyl oxygens O(a) are described as $O^{-0.4}$ ions, and thus assume the smallest charge of all oxygens. This is combined with single coordination to the Mo center directly below O(a). The asymmetric bridging oxygens O(b) are characterized as $O^{-0.6}$ by the population analysis and are only slightly more negative than the molybdenyl oxygens, which may suggest similar electronic behavior due to similar coordination involving mainly one Mo metal center. The symmetric bridging oxygens O(b′) are most negative, $O^{-0.8}$ from the populations, which indicates largest ionic contributions to the interaction with their atom neighbors. This is also true for the oxygen O(d), which corresponds to an O(b′) center of the second surface layer, and is described in its charge state by $O^{-0.8}$ from the populations.

The results from bond order analyses for the $MoO_3(010)$ based clusters (cf. Table 2), are consistent with the binding scheme suggested by the populations discussed above. The Mo–O(a) bond-order indices involving molybdenyl oxygens (1.93–1.97) are rather close to the saturation value of 2.0 which characterizes a molybdenyl double bond, in agreement with the coordination scheme. The character of the Mo–O(a) bond also becomes clear from respective charge density difference maps. Fig. 5 shows contour plots of the charge density difference $\Delta\rho(r)$ in the largest cluster, $Mo_7O_{30}H_{18}$, representing the $MoO_3(010)$ surface. Here $\Delta\rho(r)$ is defined by the difference between the self-consistent cluster charge density and that of a superposition of respective free atom charge densities. Thus, $\Delta\rho(r)$ quantifies the charge rearrangement due to bond formation in the cluster, where positive values correspond to charge accumulation and negative values to charge depletion due to binding. It is obvious from Figs. 5a and 5b that the Mo–O(a) bond formation results in charge flow from the metal center towards the oxygen (in addition to metal charge polarization), which illustrates the ionic part of the molybdenyl bond. The charge flow results also in accumulation of electron charge between the two centers, which clearly hints at covalent contributions to the bond. The increased charge about the oxygen O(a) is similar in shape to the charge distribution of an O 2sp hybrid orbital sticking out of the surface. This is to be expected, since charge accumulation at the O(a) site corresponds to an increased effective occupation of O 2p orbitals. Thus, the calculations identify a directed charge accumulation at the terminal O(a) sites which makes these centers particularly nucleophilic. A further quantification of the charge redistribution between the cluster atoms based on charge density difference maps is difficult due to the limited information given by two-dimensional representations of the three-dimensional quantity $\Delta\rho(r)$ but also because of the non-uniqueness of subdividing the total cluster charge into separate atom contributions. As a result, charge flow between atom centers evidenced visually in density difference maps is not necessarily combined with major changes in respective atom populations.

The asymmetric bridging oxygens O(b) yield Mo–O bond orders that are quite different for the two Mo centers being bridged. For Mo closest to the oxygen, values of 1.5–1.6 (denoted by Mo–O(b_1) in Table 2) show strong binding, while for Mo further away, bond orders of 0.2 (denoted by Mo–O(b_2) in Table 2) suggest only small coupling. This confirms that the oxygens O(b) are coordinated mainly to one molybdenum center, and therefore resemble the terminal molybdenyl oxygens O(a), which may be already expected from simple geometric considerations. It is further substantiated by the charge-density difference maps. Fig. 5a gives a clear indication of the similarity

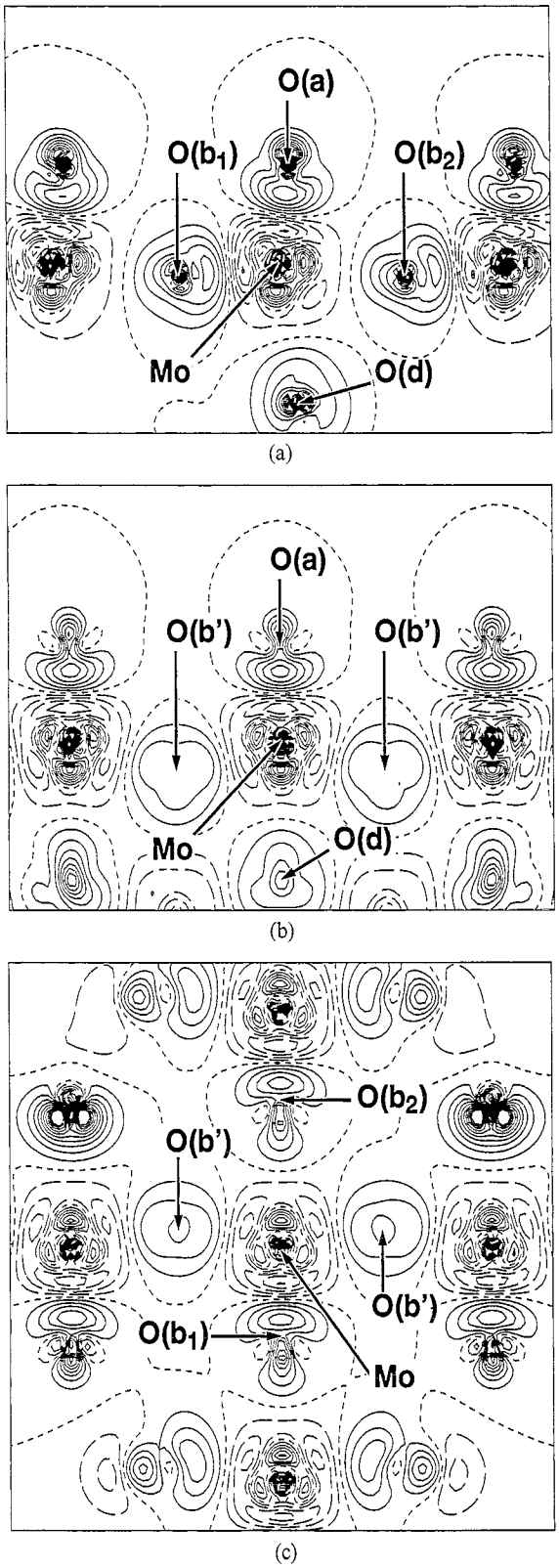

between the $O(b_1)$ and O(a) in the charge redistribution due to bond formation. In addition, Fig. 5c giving the charge density difference $\Delta\rho(r)$ in $Mo_7O_{30}H_{18}$ for a planar cut parallel to the surface illustrates the directed charge accumulation corresponding to increased 2p occupation at the bridging $O(b_1,b_2)$ centers, in analogy to the effect at the terminal O(a) sites.

Oxygens O(b′) bridging two Mo centers symmetrically result in Mo–O bond orders of 0.7–0.9 which reflect Mo–O single bonds with each of the neighboring molybdenums. Population analyses yielding O(b′) centers with highest negative charge (cf. Table 2), suggest that the Mo–O(b′) bonds are dominantly ionic. However, the charge-density difference maps of Figs. 5b and 5c suggest only small to moderate negative charge accumulation near the O(b′) sites. This discrepancy is explained by the fact that for both planar cuts shown in Figs. 5b and 5c the planes do not go through the O(b′) centers and therefore the visible charge increase does not fully reflect the actual charge accumulation. In addition, the charge increase about O(b′) is more diffuse and less directional, which emphasizes the impression of a small effect. Finally, we mention the O(d) centers, which are equivalent to O(b′) centers of the second surface layer and couple only weakly with the Mo center of the first layer, which explains the small bond order index of 0.2.

Obviously, the three different size clusters discussed above yield very similar results concerning atom charging and bond formation. This is true even for the detailed charge redistribution at the $MoO_3(010)$ surface. As an example, Fig. 6a and Fig. 6b show contour plots of the charge-density difference $\Delta\rho(r)$ in the $Mo_3O_{16}H_{14}$ cluster (Fig. 2c),

Fig. 5. Contour plots of the charge-density difference $\Delta\rho(r)$ in $Mo_7O_{30}H_{18}$ (see Fig. 2b) representing the MoO_3 (010) surface. For a definition of $\Delta\rho(r)$, see the text. The contour lines are given for a cut (a) along the (001) plane through the top most Mo, O(a), and O(b) centers, (b) along the (100) plane trough the top most Mo centers with O(a) and O(b') centers being close to the plane, and (c) along the (010) plane through the top most Mo centers. The contour values refer to increments of 0.01 au with positive values (charge accumulation) given by solid lines and negative values (charge depletion) given by long dashed lines. The zero lines are shown by short dashes.

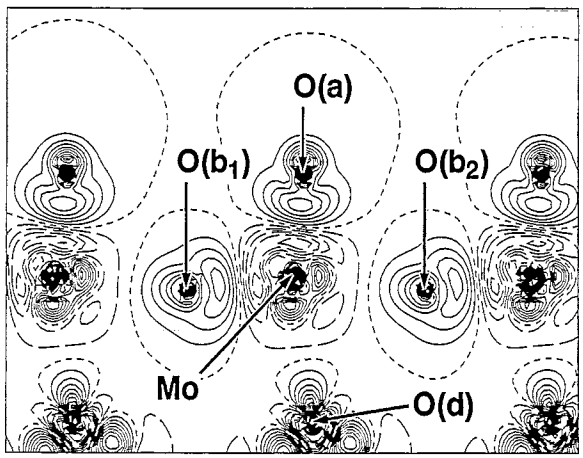

(a)

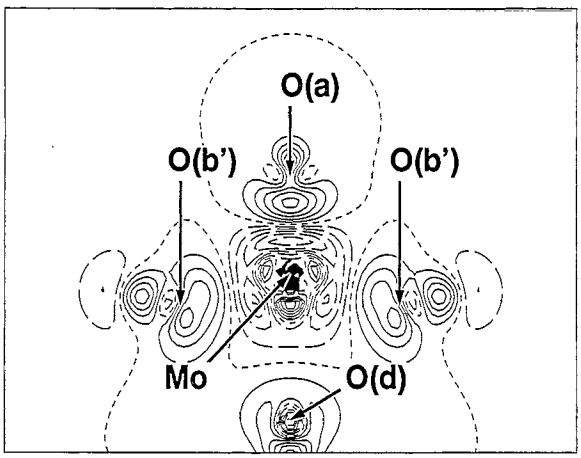

(b)

Fig. 6. Contour plots of the charge density difference $\Delta\rho(r)$ in $Mo_3O_{16}H_{14}$ (see Fig. 2c) representing the $MoO_3(010)$ surface. The contour lines are given for a cut (a) along the (001) plane through the Mo, O(a), and O(b) centers, and (b) along the (100) plane through the central Mo center with O(a), and O(b') centers being close to the plane. For contour details see Fig. 5.

which forms a subunit of the largest cluster $Mo_7O_{30}H_{18}$ (Fig. 2b). The plots of Fig. 6a and Fig. 6b refer to planar sections and contour parameters which are identical to those used for the largest cluster in Figs. 5a and 5b. A comparison of the plots shows almost no difference between the two clusters concerning the charge redistribution near the central molybdenum and the surface oxygen centers.

The agreement between the results from the differently size clusters which use the same peripheral bond saturation scheme also shows that the present saturation scheme is meaningful and leads to data which are relevant for the extended surface situation. As a further illustration, the last column of Table 2 lists population and bond-order results for the $(Mo_2O_{11}H_{13})^{3+}$ cluster (Fig. 4b) which represents the alternative peripheral bond saturation scheme mentioned in Section 2. A comparison with the data of the $Mo_2O_{11}H_{10}$ cluster (corresponding to the present saturation scheme, Figs. 2d and 4a) shows clear discrepancies. In $(Mo_2O_{11}H_{13})^{3+}$ the bridging oxygens O(b) and O(b') accumulate charge at the expense of the terminal molybdenyl oxygen, if compared with the $Mo_2O_{11}H_{10}$ results. Further, the total bond-orders of the bridging oxygens are decreased, with the decrease being most dramatic for O(b') while the bond order of the terminal molybdenyl oxygen is increased. Thus, with the alternative bond saturation scheme the asymmetric bridging oxygens are much less similar to the terminal molybdenyl oxygens, and binding of the symmetric bridging oxygens with their molybdenum neighbors is described by much smaller covalent contributions. This clearly disagrees with the results for the larger clusters. Therefore, it makes the alternative bond saturation less reasonable and stresses the use of the present scheme.

Electrostatic potentials $\Phi(r)$ computed from the cluster charge distributions can give additional information about local charging and binding at the surface. Fig. 7a shows a contour plot of $\Phi(r)$ above the $MoO_3(010)$ surface represented by the $Mo_7O_{30}H_{18}$ cluster. The plot refers to a planar cut along the (001) plane through the topmost Mo, O(a), and O(b) centers which are added as shaded spheres. The electrostatic potential $\Phi(r)$ is always found to yield negative values (contours given by long dashed lines) for distances above the surface which correspond to typical molecular binding and reaction distances. This reflects the negative charge accumulation at the surface oxygens resulting from the binding scheme discussed above. In addition, Fig. 7a shows a broad negative minimum above the leftmost terminal oxygen site O(a) (labeled "min" in the plot). This suggests that electrophilic adparticles like H^+, resulting from surface reactions, will be attracted preferentially at these sites

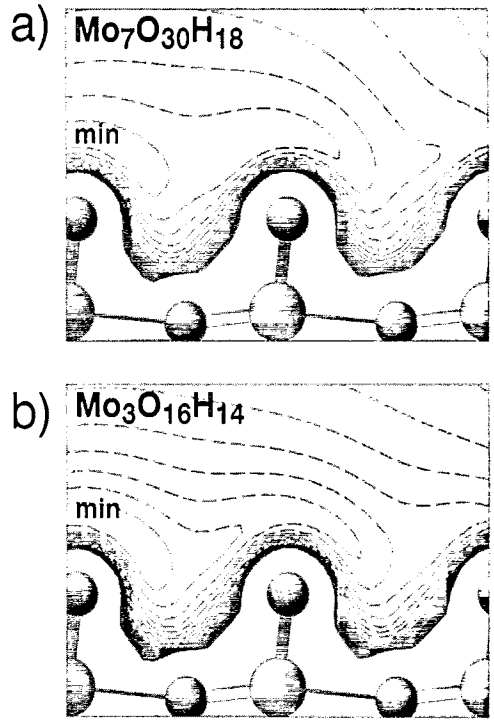

Fig. 7. Contour plots of the electrostatic potential $\Phi(r)$ about (a) the $Mo_7O_{30}H_{18}$ and (b) the $Mo_3O_{16}H_{14}$ clusters for a planar cut along the (001) plane through the topmost Mo, O(a) and O(b) centers. (The cluster centers contained in the plane are added as shaded spheres.) The contour values refer to increments of 0.01 au with positive (negative) values given by solid (long dashed) lines. The zero lines are shown by short dashes. The region of minimum potential is labeled "min".

and may form local surface bonds. However, it is not expected that the location of the smallest $\Phi(r)$ coincides with the actual binding position of the adsorbate, since the influence of covalent mixing as well as charge transfer is not included in the electrostatic potential $\Phi(r)$ of the substrate. This is confirmed by recent calculation for hydrogen adsorption on $MoO_3(010)$ discussed elsewhere [8].

The plot of Fig. 7a includes three equivalent O(a) centers where the spatial variation of $\Phi(r)$ differs somewhat between the centers. This reflects the cluster representation of the $MoO_3(010)$ surface by $Mo_7O_{30}H_{18}$ which treats the O(a) centers slightly differently. However, the qualitative result of a minimal (negative) electrostatic potential near these sites is still valid. The inequivalent treatment of the O(a) centers by the cluster approach also becomes evident in the results for the smaller clusters. As an example, Fig. 7b shows a contour plot of $\Phi(r)$ above the $MoO_3(010)$ surface represented by $Mo_3O_{16}H_{14}$ (Fig. 2c), where the plot refers to a planar section and contour parameters identical to those used for $Mo_7O_{30}H_{18}$ in Fig. 7a. A comparison of the two plots evidences very similar electrostatic potential distributions with an obvious inequivalence of the O(a) centers. This may suggest that for a more accurate description of the (long range) electrostatic surface potential $\Phi(r)$, clusters larger than those considered in the present study are required. In contrast, the results for the charge redistribution $\Delta\rho(r)$ discussed above indicated cluster-size convergence.

3.2. MoO_3 (100) *surface based clusters*

Table 3 lists calculated populations and bond orders obtained from the different surface clusters

Table 3
Populations and bond orders obtained from clusters representing the $MoO_3(100)$ surface; the geometric structures of the clusters $Mo_6O_{24}H_{12}$, $Mo_5O_{19}H_8$ and $Mo_3O_{12}H_6$ are shown in Figs. 3b–d, respectively; the population charges q and bond orders involving molybdenum refer to the two inequivalent centers of the clusters, Mo(1) and Mo(2) as shown in Fig. 3a; the inequivalent oxygen sites O(a-d) are also defined in Fig. 3a; for comparison names of the structurally equivalent oxygen centers of the $MoO_3(010)$ based clusters are added to the populations (in square brackets)

	Mo_6-$O_{24}H_{12}$	Mo_5-$O_{19}H_8$	Mo_3-$O_{12}H_6$
Populations			
Mo(1)	40.36	40.52	40.59
Mo(2)	40.38	40.37	40.38
O(a) [≈O(b_1) on (010)]	8.39	8.39	8.40
O(d_1) [≈O(a) on (010)]	8.37	8.38	8.39
O(d_2) [≈O(a) on (010)]	8.40	8.40	8.39
O(b'_1) [≈O(b′) on (010)]	8.88	8.88	8.86
O(b'_2) [≈O(b′) on (010)]	8.83	8.85	8.85
Bond orders			
Mo(1)-O(d_1)	1.95	1.95	1.96
Mo(1)-O(b'_1)	0.23	0.22	0.26
Mo(1)-O(b'_2)	0.66	0.64	0.59
Mo(2)-O(a)	1.94	1.96	1.96
Mo(2)-O(d_2)	1.95	1.96	2.00
Mo(2)-O(b'_1)	0.55	0.55	0.57
Mo(2)-O(b'_2)	0.19	0.18	0.20

$Mo_6O_{24}H_{12}$, $Mo_5O_{19}H_8$ and $Mo_3O_{12}H_6$, representing the $MoO_3(100)$ surface. Analogous to the cluster results for the $MoO_3(010)$ surface (cf. Table 2) the data vary only slightly between the three differently sized clusters which confirms the validity of the cluster approach for the present system. The populations of the $MoO_3(100)$-derived clusters are also rather similar to those of the $MoO_3(010)$ clusters discussed previously. The Mo metal centers can be described as positively charged $Mo^{+(1.4-1.6)}$ ions from the populations. The terminal molybdenyl oxygens O(a) (corresponding to the asymmetric bridging O(b) centers in the $MoO_3(010)$ based clusters, but with the farther of the two molybdenum neighbors missing, see $O(b_1)$ in Fig. 2a) accumulate only little charge, becoming $O^{-0.4}$ ions, which is combined with their single coordination to the Mo center directly below. The bridging oxygens $O(d_1,d_2)$ (corresponding to the terminal O(a) centers in the $MoO_3(010)$ based clusters, see Fig. 2a) are also described as $O^{-0.4}$ ions and are therefore similar to the terminal O(a) centers, which is explained by their similarity in structure and coordination. The bridging oxygens $O(b'_1,b'_2)$ (corresponding to the symmetric bridging O(b') centers in the $MoO_3(010)$ based clusters, see Fig. 2a) are most negative, $O^{-0.85}$ from the populations indicating major ionic interaction with their atom neighbors. Altogether, the oxygen centers of the $MoO_3(100)$ based clusters differ very little in their populations from those of the $MoO_3(010)$ based clusters if structurally equivalent centers are compared. This suggests that charging of the atom centers is determined by the bulk structure rather than by the specific orientation of the ideal surface.

The bond-order analyses for the $MoO_3(100)$ based clusters (cf. Table 3), also yield very similar results compared with those of the $MoO_3(010)$-based clusters (cf. Table 2). Both the $Mo(1)–O(d_1)$ and $Mo(2)–O(d_2)$ bonds of the (100) surface involve terminal (molybdenyl) oxygens and correspond structurally to the Mo–O(a) molybdenyl bond at the $MoO_3(010)$ surface. This explains that the respective bond order indices (1.95–2.00) are close to the saturation value characterizing a molybdenyl double bond, in agreement with the bond order of the Mo–O(a) bonds on $MoO_3(010)$. The Mo(2)–O(a) bonds of the (100) surface also involve terminal oxygens, and their bond orders (1.95) describe molybdenyl double bonds. These bonds are structurally connected with the asymmetric bridging oxygen bonds, $Mo–O(b_1)$, where, however, one Mo bridging partner (the Mo furthest away) is missing. As a consequence, the bond order of the Mo(2)–O(a) bond on $MoO_3(100)$ is found to be larger than that of the $Mo–O(b_1)$ bond on $MoO_3(010)$.

The nature of the Mo(2)–O(a), $Mo(1)–O(d_1)$ and $Mo(2)–O(d_2)$ bonds involving terminal oxygens on $MoO_3(100)$ can be shown by respective charge-density difference $\Delta\rho(r)$, maps. Fig. 8 gives contour plots of $\Delta\rho(r)$ in the largest cluster, $Mo_6O_{24}H_{12}$, representing the $MoO_3(100)$ surface where all contour parameters are identical to those of Figs. 5 and 6. Obviously, the formation of all three Mo–O bonds involving terminal oxygens is combined with charge flow from the metal towards the oxygen center, which illustrates the ionic part of the molybdenyl bond. Furthermore, there is some charge accumulation between the two centers which suggests covalent binding contributions. The shape of the charge rearrangement in the bond region is quite similar in all three cases and resembles that of the Mo–O(a) bond on $MoO_3(010)$ very closely (cf. Fig. 5a). The increased charge about the terminal oxygens is qualitatively described by the charge distribution of O 2sp hybrid orbitals sticking out at the oxygen end of the bond, which reflects the increased effective O 2p occupation due to charge transfer. Therefore, the calculations indicate for all three bonds a directed charge accumulation at the terminal oxygens, which makes them possible candidates for nucleophilic centers.

The two inequivalent bridging oxygens $O(b'_1)$ and $O(b'_2)$ on $MoO_3(100)$ correspond structurally to symmetric bridging oxygens O(b') on $MoO_3(010)$. This is confirmed by respective Mo–O bond order results. The $Mo(1)–O(b'_2)$ and $Mo(2)–O(b'_1)$ bonds pointing along the symmetric bridges yield bond orders of 0.55–0.65 (cf. Table 3), which suggests Mo–O single bonds with each of the neighboring molybdenums. This agrees well with the bond-order result for Mo–O(b') bonds on $MoO_3(010)$. Table 3 includes also bond orders

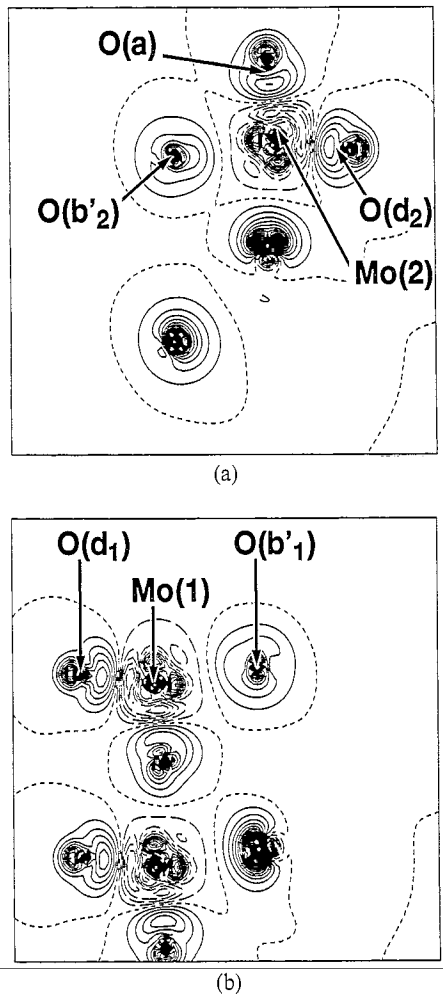

Fig. 8. Contour plots of the charge density difference $\Delta\rho(r)$ in $Mo_6O_{24}H_{12}$ representing the $MoO_3(100)$ surface. The contour lines are given for a cut along the (001) plane (a) through the Mo(2), O(a), O(b'$_2$), and O(d$_2$) centers, and (b) through the Mo(1), O(b'$_1$) and O(d$_1$) centers. For contour details see Fig. 5.

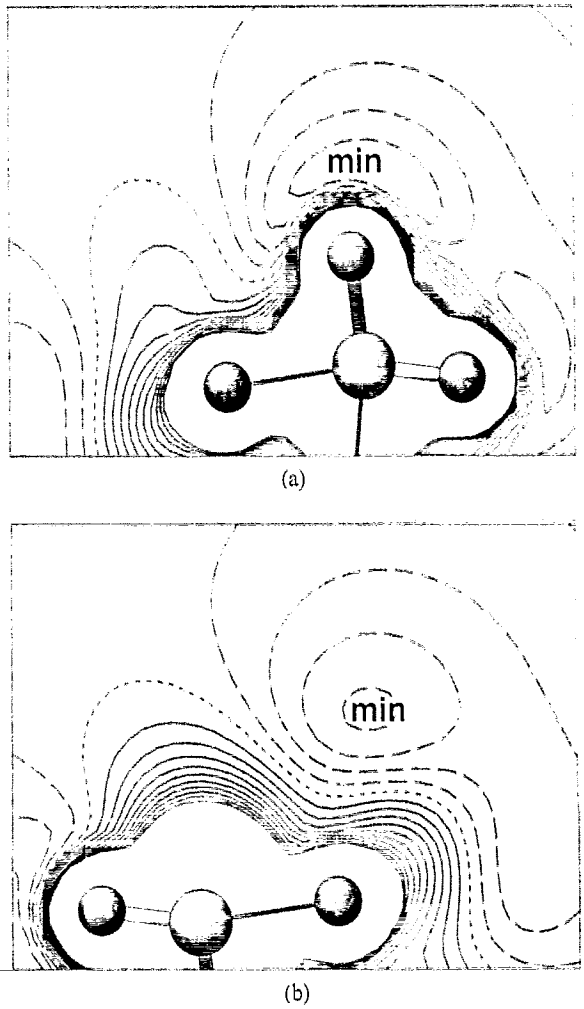

Fig. 9. Contour plots of the electrostatic potential $\Phi(r)$ about the $Mo_6O_{24}H_{12}$ cluster for cuts along the (001) plane (a) through the Mo(2), O(a), O(b'$_2$) and O(d$_2$) centers, and (b) through the Mo(1), O(b'$_1$) and O(d$_1$) centers. (The cluster centers contained in the plane are added as shaded spheres.) For contour details see Fig. 7. The region of minimum potential is labeled "min" in each plot.

for the Mo(1)–O(b'$_1$) and Mo(2)–O(b'$_2$) bonds which belong to the longest bond distances in the clusters and correspond to the weak Mo–O(d) bonds on MoO_3(010). As a consequence, the bond orders assume quite small values of 0.2, characterizing weak coupling as expected.

Fig. 9 shows contour plots of the electrostatic potential $\Phi(r)$ above the MoO_3 (100) surface represented by the $Mo_6O_{24}H_{12}$ cluster. The plots are given for two parallel planar cuts along the (001) plane (Fig. 9a) through the Mo(2), O(a), O(b'$_2$), and O(d$_2$) centers, and (Fig. 9b) through the Mo(1), O(b'$_1$), and O(d$_1$) centers (added as shaded spheres, see Fig. 3a). The potential $\Phi(r)$ yields negative values (contours given by long dashed lines) with a broad minimum (labeled "min" in the plot) at typical molecular binding and reaction distances above the terminal oxygens O(a) (see Fig. 9a), which reflects the directed negative charge accumulation near these centers. The minimum potential region extends along the (001) direction connecting the terminal oxygens O(a), which

becomes evident from Fig. 9b. Here $\Phi(r)$ is given for a cut between the O(a) centers and yields a potential minimum whose height and lateral position is fairly close to that of Fig. 9a. In addition, Fig. 9b shows that above the bare metal center Mo(1), the electrostatic potential $\Phi(r)$ assumes only positive or very small negative values which is also true for regions above the oxygens $O(b'_2)$ which bridge the Mo(1) centers. Altogether, this yields a qualitatively simple potential variation which suggests that electrophilic adparticles, like H^+, resulting from surface reactions will be attracted at or between adjacent molybdenyl oxygens O(a), but not near bare metal sites.

4. Conclusions

The present cluster model calculations yield electronic parameters which are converged with respect to cluster size and can therefore give a clear picture of the electronic structure and binding near the different oxygen sites at the MoO_3(010) and (100) surfaces. The ionic nature of the MoO_3 compound is confirmed by the calculations, and populations as well as bond orders show characteristic differences for geometrically inequivalent oxygens. Terminal molybdenyl oxygens accumulate the smallest negative charge (−0.4) and their interaction with the environment is described by a double bond with the adjacent Mo center. Asymmetric bridging oxygens are slightly more negative (−0.5) and are characterized by a binding scheme similar to that for the molybdenyl oxygens. Symmetric bridging oxygens become most negative (−0.8) and their binding behavior is described by single bonds with the two neighboring Mo centers. Electrostatic potentials determined from cluster charge distributions show broad negative minima above the terminal oxygens, while there are no minima above bare Mo metal centers which can affect stabilization and binding as well as the reaction of electrophilic adparticles at the MoO_3 surfaces.

The cluster results of electronic parameters obtained for geometrically equivalent oxygens of the two surface orientations are found to be very similar and do not seem to depend strongly on the surface geometry. Therefore, the electronic structure at the ideal MoO_3(010) and (100) surfaces is determined mainly by their detailed atom arrangement and is not influenced by major charge redistributions due to substrate surface binding. This result suggests that the electronic behavior of the present surface systems may be decomposed into two independent components. The first component accounts for local electronic properties of the different oxygen and metal ions which depend on the local atom environment but not on the global surface geometry/orientation. The second component is represented by purely geometric factors determining the detailed surface geometry. The latter can be described (apart from a strict definition by absolute atom positions) by quantities such as the relative concentration of surface oxygens and their number of inequivalent sites, the presence/absence of bare metal ion sites at the surface, and the surface compactness. Possible relaxations and reconstruction at the real MoO_3 surfaces which are neglected in the theoretical study but indicated by the experiment [5], may change quantitative details of present results but are expected to leave the general binding picture valid. Overall, the present cluster results can give a simple description of interatomic binding and charging at the MoO_3(010) and (100) surfaces, which forms a sound basis for detailed studies on adsorbate binding and reactions [8].

Acknowledgements

Financial support by the Polish Academy of Sciences and Deutsche Forschungsgemeinschaft as well as by the Stiftung für Deutsch–Polnische Zusammenarbeit (Proj. No. 1279/94/LN) is gratefully acknowledged. One of the authors (A.M.) thanks the Fritz–Haber–Institut der Max–Planck–Gesellschaft for a stipend, as well as the COST D3 project from the Commission of the European Communities for the travel support. Furthermore, the authors would like to thank Profs. J. Haber and B. Delmon for stimulating discussions.

References

[1] H.K. Kung, Transition-metal Oxides: Surface Chemistry and Catalysis, Studies in Surface Science and Catalysis, Vol. 45, Eds. B. Delmon and J.T. Yates (Elsevier, Amsterdam, 1989).
[2] O.V. Krylov and V.F. Kiselev, Adsorption and Catalysis on Transition-metals and Their Oxides, Eds. G. Ertl and R. Gomer (Springer, New York, 1989).
[3] A. Bielanski and J. Haber in: Oxygen in Catalysis (Marcell Dekker, New York, 1991).
[4] S. Yoshida, S. Sakaki and H. Kobayashi, Electronic Processes in Catalysis: A Quantum Chemical Approach to Catalysis (VCH, New York, 1994).
[5] See E.R. Braithwaite and J. Haber (Eds.), Molybdenum: An Outline of its Chemistry and Uses, Studies in Inorganic Chemistry, Vol. 19 (Elsevier, Amsterdam, 1994).
[6] J.C. Volta and J.L. Portefaix, Appl. Catal. 18 (1985) 1.
[7] J.C. Volta and J.M. Tatibouet, J. Catal. 93 (1985) 467.
[8] A. Michalak, M. Witko and K. Hermann, to be published.
[9] L. Kihlborg, Arkiv. Kemi. 21 (1963) 357.
[10] See G. Pacchioni, P.S. Bagus and F. Parmigiani, Eds., Cluster Models for Surface and Bulk Phenomena, NATO ASI Series B, Vol. 283 (Plenum, New York, 1992).
[11] E. Broclawik, Proc. Jpn. Catal. Soc. Meeting, Kagoshima 1994, private communication.
[12] See J.K. Labanowski and J.W. Anzelm, Eds., Density Functional Methods in Chemistry (Springer, New York, 1991).
[13] N. Godbout, D.R. Salahub, J. Andzelm and E. Wimmer, Can. J. Phys. 70 (1992) 560.
[14] J. Andzelm, E. Radzio and D.R. Salahub, J. Chem. Phys. 83 (1985) 4573.
[15] The DFT–LCGTO– program package DeMon was developed by A. St-Amant and D. R. Salahub at the University of Montreal.
[16] S.H. Vosko, L. Wilk and M. Nusair, Can. J. Phys. 58 (1980) 1200.
[17] M. Witko and K. Hermann, J. Electron Spectrosc. Relat. Phenom. 69 (1994) 89.
[18] R.S. Mulliken, J. Chem. Phys. 23 (1955) 1833; 1841; 2388; 2343.
[19] I. Mayer, Chem. Phys. Lett. 97 (1983) 270.
[20] I. Mayer, J. Mol. Struct. (Theochem) 149 (1987) 81.
[21] R. Bonaccorsi, E. Scrocco and J. Tomasi, J. Chem. Phys. 52 (1970) 5270.